

Article

Calculation of the Height of the Water-Conducting Fracture Zone Based on the Analysis of Critical Fracturing of Overlying Strata

Yi Tan ^{1,2,3}, Hao Cheng ^{1,2}, Wenyu Lv ³, Weitao Yan ^{2,*}, Wenbing Guo ^{1,2}, Yujiang Zhang ⁴, Tingye Qi ⁴, Dawei Yin ⁵, Sijiang Wei ^{1,2}, Jianji Ren ² and Yajun Xin ¹

- ¹ School of Energy Science and Engineering, Henan Polytechnic University, Jiaozuo 454000, China; tanyi@hpu.edu.cn (Y.T.); hpuchenghao@163.com (H.C.); guowb@hpu.edu.cn (W.G.); weisj@hpu.edu.cn (S.W.); xinyj2007@163.com (Y.X.)
- ² State Collaborative Innovation Center of Coal Work Safety and Clean-Efficiency Utilization, Henan Polytechnic University, Jiaozuo 454000, China; renjianji@hpu.edu.cn
- ³ State Key Laboratory of Coal Resources in Western China, Xi'an University of Science and Technology, Xi'an 710054, China; lvwenyu@xust.edu.cn
- ⁴ College of Mining Engineering, Taiyuan University of Technology, Taiyuan 030024, China; ylczyj@yeah.net (Y.Z.); qty198402@163.com (T.Q.)
- ⁵ College of Energy and Mining Engineering, Shandong University of Science and Technology, Qingdao 266000, China; yindawei@sdust.edu.cn
- * Correspondence: yanweitao@hpu.edu.cn; Tel.: +86-136-9391-2813



Citation: Tan, Y.; Cheng, H.; Lv, W.; Yan, W.; Guo, W.; Zhang, Y.; Qi, T.; Yin, D.; Wei, S.; Ren, J.; et al. Calculation of the Height of the Water-Conducting Fracture Zone Based on the Analysis of Critical Fracturing of Overlying Strata. *Sustainability* **2022**, *14*, 5221. <https://doi.org/10.3390/su14095221>

Academic Editors: Cun Zhang, Fangtian Wang, Shiqi Liu and Erhu Bai

Received: 18 March 2022

Accepted: 22 April 2022

Published: 26 April 2022

Publisher's Note: MDPI stays neutral with regard to jurisdictional claims in published maps and institutional affiliations.



Copyright: © 2022 by the authors. Licensee MDPI, Basel, Switzerland. This article is an open access article distributed under the terms and conditions of the Creative Commons Attribution (CC BY) license (<https://creativecommons.org/licenses/by/4.0/>).

Abstract: Accurate division of the water-conducting fracturing zone (WCFZ) in the mining overburden serves as an important basis to evaluate the stability of coal mining under water bodies. Research on the WCFZ is conducive to controlling surface subsidence and realizing safe coal mining under water. Traditionally, the WCFZ is generally determined by field observation (liquid leakage method, borehole television, etc.) or empirical formula. Although these methods boast high accuracy, they are time-consuming and laborious and have some problems such as weak pertinence and a large value range. In this study, a mechanical model under the critical breakage condition of hard and soft strata was established on the basis of the specific geological and mining information of a mine. Besides, the stability condition for the broken strata to form the “masonry beam” structure and the deflection-based bending deformation formula of hard and soft strata were deduced, and the method of calculating the height of WCFZ based on the analysis of critical fracturing of soft and hard strata (hereafter referred to as the CFSHS-based height calculation method) was proposed. Furthermore, with reference to the results of specific engineering tests, the height of the WCFZ in the working face 15,101 of coal mine XJ was analyzed by means of theoretical analysis, numerical simulation and engineering verification, which verifies the rationality and practicability of the CFSHS-based height calculation method.

Keywords: water-conducting fracture zone; height calculation method; critical fracturing; mechanical model

1. Introduction

Coal mining destroys the equilibrium state of the overburden on the stope, resulting in a series of strata movements such as bending, fracture and caving of overburden. Eventually, the stope is vertically divided into a caving zone, a fracture zone and a bending subsidence zone, collectively called the “three zones”. The caving zone and the fracture zone belong to the water-conducting fracture zone (WCFZ) [1–3]. A series of stratum movements induced by coal seam mining can cause certain harm to the environment, which directly leads to surface collapse, soil erosion, and surface building damage [4,5]. With respect to the above problems, Peng et al. put forward the stratum control theory

and controlled strata by studying the law of overburden movement induced by coal seam mining [1]. Fan et al. proposed the concept of water conservation coal mining. Afterwards, scholars have carried out a series of theoretical researches accordingly [6]. Accurate division of the WCFZ in the mining overburden serves as an important basis to evaluate the stability of coal mining under water bodies [7]. Therefore, it is of great significance to accurately evaluate the development of the WCFZ in the mining overburden for safe mining.

Researches on the WCFZ in the mining overburden generally adopted the methods of on-site measurement, numerical simulation, physical simulation and micro-seismic monitoring [8–14]. Xu et al. explored the influence of the position of the main key stratum on the development height of the WCFZ; they proposed the conditions to adopt the empirical equation from the perspective of the position of the main key stratum. Moreover, on this basis, they found a method to predict the height of the WCFZ based on the position of the key stratum [15,16]. Peng et al. held that the caving zone and the fracture zone were 2–8 times and 30–50 times as thick as the mining height, respectively [17]. Guo et al. discussed the process of overburden failure in detail and put forward a new method to calculate the height of WCFZ based on the process of overburden failure migration [18]. Fan et al. studied the development characteristics of the WCFZ through on-site measurement and physical simulation; they revealed the dynamic evolution characteristic of “development-development-closure” of the mining-induced fractures and discovered the “mud cap effect” revealed by mining failure under thick mud caprock [6]. Wang et al. proposed a new method and its applicable conditions for the division of the “vertical three zones” of mining overburden based on the key stratum stability and the characteristics of post-fracture movement through physical simulation experiments and the key stratum theory [19,20]. These studies provide good ideas for dividing the WCFZ in the mining overburden under general geological conditions and traditional mining conditions.

With respect to the composite structure of hard and soft strata, this study analyzed the critical condition for the breakage of hard and soft strata, put forward a theoretical judgment method and its applicable conditions for the division of the WCFZ based on strata deflection and bending deformation of the overburden composite structure. Then, this theoretical judgment method, numerical simulation method and engineering analogy method were applied to the division of the WCFZ in the mining overburden, and the rationality of this method was verified by comparing the results with the on-site measurement results.

2. Mining Overburden Structure and Mechanical Analysis

2.1. Determination of the Bearing Strata

In the stope overburden, the thick hard rock plays the bearing role while the thin soft rock plays the loading role. According to the stratum occurrence conditions, the load value and stratum of hard rock are calculated by Equations (1) and (2). From bottom to top, it is named the i -th hard stratum ($i = 1, 2, 3, \dots$):

$$q_1(x)|_m = \frac{E_1 h_1^3 \sum_{i=1}^m \gamma_i h_i}{\sum_{i=1}^m E_i h_i^3} \quad (1)$$

$$q_1(x)|_m > q_1(x)|_{m+1} \quad (2)$$

where $q_1(x)|_m$ is the load borne by the first hard stratum for the m -th stratum, MPa; E_i is the elastic modulus of the i -th stratum, MPa; h_i is the thickness of the i -th stratum, m; γ_i is the unit weight of the i -th stratum, MN/m³.

2.2. Mechanical Analysis on the Hard Rock Strata

2.2.1. Analysis on the Stability of the “Masonry Beam” Structure

With the continuous advancement of the working face, the upper strata exceed the maximum suspending length and breaks, forming neatly arranged rock blocks which squeeze each other to form a masonry beam structure which resembles a beam yet is an arch in essence. Blocks B and C in the “masonry beam” structure are called key blocks

whose stability determines the stability of the whole “masonry beam” structure (Figure 1). Based on the instability form of key blocks, the masonry beam structure falls into sliding instability and rotary deformation and instability [21–24].

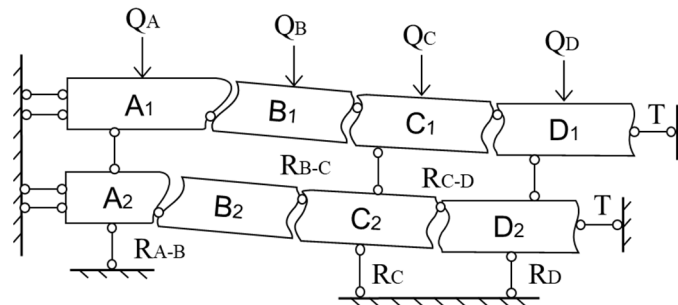


Figure 1. Schematic diagram of the “masonry beam” structure where $A_1, B_1, C_1, D_1, A_2, B_2, C_2$ and D_2 are articulated rock blocks; R is the jointing force and supporting force between rock blocks; T is the horizontal thrust for the structure; q is the load.

① Sliding instability

The condition where no sliding instability of key blocks in the “masonry beam” occurs is:

$$i \leq \tan \varphi + \frac{3}{4} \sin \theta \quad (3)$$

where $i = h/L_z$; h is the stratum thickness, m ; L_z is the length of the periodically broken block, m ; φ is the friction angle between broken blocks; θ is the rotary angle between the key blocks, $^\circ$.

The condition where no sliding instability of this structure occurs is directly related to the block size i and the rotary angle.

② Rotary deformation and instability

The conditions where no rotary deformation and instability of key blocks in the “masonry beam” occurs are:

$$\frac{P}{\left(i - \frac{1}{2} \sin \theta\right) (i - \sin \theta)} \leq 0.15 \sigma_c \quad (4)$$

P is the load borne by the key block, MN ; σ_c is compressive strength of the bearing stratum, MPa ;

$$L_z = h \sqrt{\frac{\sigma_t}{3q}} \quad (5)$$

$$\Delta = M - \sum h(K_p - 1) \quad (6)$$

$$\sin \theta = \frac{\Delta}{L_z} \quad (7)$$

where σ_t is the tensile strength of the stratum, MPa ; q is the load borne by the stratum, MPa ; Δ is the height of the free space below the stratum, m ; M is the thickness of the mining coal seam, m ; K_p is the dilatancy coefficient of the stratum.

2.2.2. Analysis on the Bending Subsidence Deformation of the Hard Strata

The maximum stratum subsidence deformation is related to the height of cavity below it, which determines whether the stratum is damaged [25–28]. The stratum without initial breakage is regarded as a fixed-beam model with fixed ends (Figure 2) [29]. The tensile strength served as the stratum failure criterion; then the deflection Equation (10) and the stratum maximum subsidence (11) under the critical failure condition of the stratum are obtained [30,31].

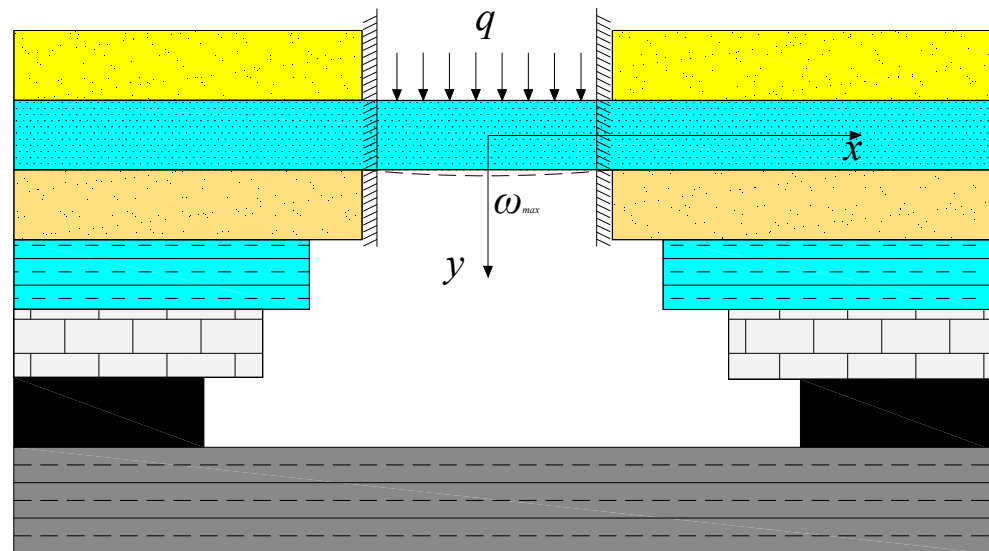


Figure 2. Model of the first breakage of strata.

According to the calculation of the first breakage model, when the normal stress of the stratum reaches the tensile strength, the stratum is cracked.

$$L_c = h \sqrt{\frac{2\sigma_t}{q}} \quad (8)$$

$$I = \frac{bh^3}{12} \quad (9)$$

where L_c is the length of the initial broken block, m; I is the moment of inertia of the rectangular section of the beam, m^4 ; b is the width of the rectangular section of the beam, m.

When the width of the rectangular section of the stratum is unit width, i.e., $b = 1$:

$$\omega(x) = \frac{q}{24EI} \left(x^2 - \frac{1}{4}L_c^2 \right)^2 \quad (10)$$

where ω is the beam deflection, m; E is the elastic modulus of the stratum, MPa.

When $x = 0$, the bending deformation of the fixed beam reaches its maximum value:

$$\omega_{max} = \frac{qL_c^4}{384EI} = \frac{h\sigma_t^2}{8Eq} \quad (11)$$

2.3. Mechanical Analysis on the Soft Strata

When the horizontal tensile strain under load exceeds the tensile strain, the soft stratum breaks:

$$\varepsilon_{max} = \frac{3ql^2}{8Eh^2} > \frac{\sigma_t}{E} \quad (12)$$

where ε_{max} is the horizontal tensile strain.

$$l_S = h \sqrt{\frac{8\sigma_t}{3q}} \quad (13)$$

$$\omega = \frac{5ql^4}{32Eh^3} \quad (14)$$

where l_S is the breaking length of the soft stratum, m; ω is its corresponding deflection of the soft stratum, m.

The breakage of the soft stratum requires the following two conditions: (1) the horizontal tensile strain generated by loading is greater than its tensile strain; (2) the corresponding deflection of the soft stratum is smaller than the height of the free space below.

$$\frac{3ql^2}{8Eh^2} > \frac{\sigma_t}{E} \quad (15)$$

$$\frac{5ql^4}{32Eh^3} < M - \sum h_i((K_p)_i - 1) \quad (16)$$

where M is the thickness of the mining coal seam, m ; h_i is the thickness of the i -th stratum, m ; $(K_p)_i$ is the residual dilatancy coefficient of the i -th stratum.

3. CFSHS-Based Height Calculation Method

Based on the above bearing stratum judgment, the specific analysis on the stability of the "masonry beam" structure and the stratum bending and subsidence deformation, the method of calculating the height of WCFZ based on the analysis of critical fracturing of soft and hard strata (hereafter referred to as the CFSHS-based height calculation method) was proposed. The specific calculation procedure is as follows:

Step 1: According to the above bearing stratum judgment method, the load borne by the hard stratum and its stratum position are determined. From bottom to top, it is named the i -th hard stratum ($i = 1, 2, 3, \dots$). The soft stratum borne by it is named the (i, j) soft stratum from bottom to top (i is number of the corresponding hard stratum; $j = 1, 2, 3, \dots$).

Step 2: With reference to the thickness of the mining coal seam, the height between the stratum and the coal seam, as well as the dilatancy characteristics of the stratum, the height of the free space Δ_i below the stratum is calculated according to Equation (12):

$$\Delta_i = M - \sum h_i((K_p)_i - 1) \quad (17)$$

where Δ_i is the height of the free space below the i -th stratum, m ; M is the thickness of the mining coal seam, m ; h_i is the thickness of the i -th stratum, m ; $(K_p)_i$ is the residual dilatancy coefficient of the i -th stratum.

Step 3: Based on the thickness, tensile strength and bearing load of the hard stratum, the broken block length $(Lz)_i$ of the i -th hard stratum is calculated with reference to Equation (5). The rotary angle of the i -th hard stratum θ_i is calculated with reference to the height of the free space below the stratum and Equation (7).

Step 4: The tensile strength, bearing load and thickness of the hard stratum are substituted into Equation (11) to obtain the maximum bending deformation value of the hard stratum $(\omega_{max})_i$, which is then compared with the height of the free space below it Δ_i :

$$\Delta_i \leq (\omega_{max})_i \quad (18)$$

If Equation (18) is valid, i.e., the height of the free space below the stratum is smaller than its maximum bending deformation value, it is determined that the stratum does not break, only bending deformation occurs, and the stratum is the lower boundary of the bending subsidence zone. Otherwise, if Equation (18) is invalid, i.e., the height of the free space below the stratum is greater than its maximum bending deformation value, the parameters including the rotary angle obtained in Step 3 are substituted into Equations (3) and (4) for judgment. When Equations (3) and (4) are invalid at the same time, the hard stratum belongs to the caving zone. When Equations (3) and (4) are valid at the same time, the hard stratum breaks, and the overburden failure continues to develop upward to the soft stratum which it bears.

Step 5: Determination is made according to the elastic modulus, tensile strength, stratum bearing load and thickness of the (i, j) soft stratum in combination with Equations (15) and (16).

If Equations (15) and (16) are valid at the same time, i.e., when the horizontal tensile strain generated by the loading of the (i, j) soft stratum is greater than its tensile strain limit and the deflection corresponding to the soft stratum is smaller than the height of the free space below it, the soft stratum breaks and the fracture continues to develop upward. Otherwise, the fracture development stops. Analysis is made stratum by stratum accordingly; then the unfractured stratum is found. The height from the stratum to the coal seam roof is the height of the WCFZ.

The following two conditions are the prerequisites for applying the theoretical judgment method: (1) The working face reaches the overburden failure and full mining in the advancing direction, that is, the height of the WCFZ no longer increases with the advancement of the working face. (2) The lithology, stratum thickness and mechanical parameters of the overburden of the working face are fully grasped.

4. Engineering Case Analysis

4.1. Geological Overview

Coal Mine XJ, which belongs to Changzhi Xinjian Coal Industry Co., Ltd., is located in the west of Nansong Town which is 15 km away in the south of Shangdang district in Changzhi city. The main coal seam in the mine field is coal seam 15, located at the bottom of Taiyuan Group, 98.86 m above coal seam 3, with an average thickness of 4.20 m. It has a simple structure and its whole area is recoverable. The coal seam roof is limestone; the floor is mudstone and sandy mudstone. The histogram of the overburden is given in Figure 3.

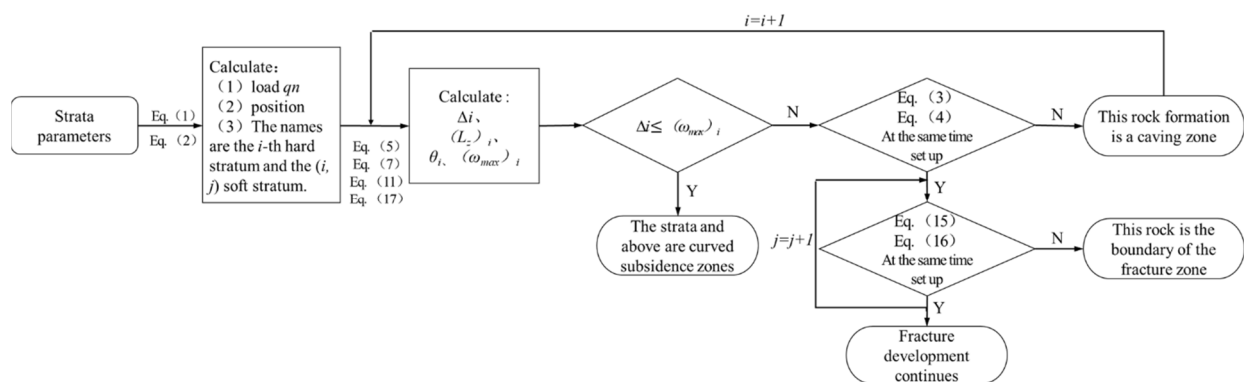


Figure 3. CFSHS-based height calculation method.

This study designs to observe the working face 15,101 which has a strike length of about 1400 m, an inclined length of about 176 m, a horizontal elevation of +849–920 m, a coal seam dip angle of 0–8° and a buried depth of about 276.88 m. The comprehensive mechanized mining is adopted with a mining height of 4.2 m and an advancing speed of 3.6 m/d, and the overburden reaches the fully mining state in the advancing direction.

The normal water inflow of working face 15,101 is 9.19 m³/h, and the maximum daily water inflow is 16.9 m³/h. It is the largest from June to August and the smallest from January to April, which is directly related to rainfall. The hydrogeological type is medium. Most of the surface is exposed bedrock and partially covered by Quaternary loess. The complexity of mine field structure is a simple type. In coal seam 3, there is no large geological structure and large geological events.

According to the on-site test, the dilatancy coefficient K_z of the immediate roof in the goaf of working face 15,101 is 1.15; the residual dilatancy coefficient of the upper rock stratum gradually decreases in the logarithmic form. According to researches [32,33], the relationship between the average residual dilatancy coefficient K_p of the stratum and the mining distance from the coal seam h is:

$$K_p = K_z - 0.017 \ln h (h < 100 \text{ m}) \quad (19)$$

When $h > 100$ m, the upper stratum on the working face is hard stratum, which is broken in large blocks and neatly arranged, with a small residual dilatancy coefficient K_z . Calculation reveals that the average residual dilatancy coefficient of the 16th stratum (mudstone) at a mining distance of 98.86 m from the coal seam is 1.07, so the average residual dilatancy coefficient of the 17th stratum and its upper strata shall be smaller than 1.07; hence both are set as 1.06.

The thickness and mechanical parameters of strata can be obtained from the geological drilling data of the working face (Figure 4).

Number	Column	Lithology	Thickness(m)	Buried depth(m)	Bulk density (kg·m ⁻³)	Tensile strength(Mpa)	Compressive strength(Mpa)	Elastic modulus(Gpa)	Volume expansion coefficient
30		Quaternary strata	27.85	27.85	1832	0.024	0.192	33.42	1.06
29		Medium sandstone	6.25	34.10	2345	7.01	56.08	19.49	1.06
28		Fine sandstone	8.95	43.05	2319	8.41	67.28	21.13	1.06
27		Sandy mudstone	12.95	56.00	2670	5.43	43.44	18.35	1.06
26		Siltstone	12.20	68.20	2657	4.52	36.16	23.64	1.06
25		Medium sandstone	14.95	83.15	2564	6.14	49.12	29.62	1.06
24		Sandy mudstone	8.80	91.95	2541	5.14	41.12	18.46	1.06
23		Mudstone	26.10	118.05	2432	6.28	50.24	18.66	1.06
22		Medium sandstone	15.85	133.90	2274	6.57	52.56	22.41	1.06
21		Siltstone	13.81	147.71	2560	4.45	35.6	21.54	1.06
20		Sandy mudstone	9.37	157.08	2432	4.78	38.24	19.44	1.06
19		Siltstone	4.35	161.43	2521	4.62	36.96	21.09	1.06
18		Sandy mudstone	12.75	174.18	2630	4.66	37.28	18.56	1.06
17		3# coal	3.84	178.02	1102	1.27	10.16	8.45	1.06
16		Mudstone	12.39	190.41	2345	5.99	47.92	22.07	1.07
15		Siltstone	4.80	195.21	2568	4.61	36.88	23.17	1.07
14		Sandy mudstone	9.48	204.69	2577	4.14	33.12	19.66	1.08
13		Limestone	5.20	209.89	2432	5.17	41.36	27.46	1.08
12		Mudstone	4.13	214.02	2352	6.18	49.44	21.54	1.08
11		Siltstone	7.53	221.55	2671	4.37	34.96	24.88	1.08
10		Fine sandstone	5.77	227.32	2754	7.93	63.44	28.94	1.08
9		Siltstone	8.38	235.70	2530	7.89	56.7	24.77	1.08
8		Fine sandstone	5.98	241.68	2789	8.11	64.88	30.44	1.09
7		Limestone	3.25	244.93	2451	5.63	45.04	25.62	1.09
6		Fine sandstone	2.87	247.80	2741	7.65	61.2	29.51	1.09
5		Mudstone	7.49	255.29	2563	6.21	49.68	20.11	1.09
4		Limestone	4.79	260.08	2511	5.89	47.12	28.17	1.10
3		Sandy mudstone	3.17	263.25	2649	5.84	46.72	18.35	1.10
2		Mudstone	6.13	269.38	2411	5.86	46.88	19.45	1.11
1		Limestone	7.50	276.88	2569	6.33	50.64	27.44	1.15
0		15# coal	4.20	281.08	1330	6.10	7.56	5.04	/
Floor		Mudstone	2.81	283.89	2496	5.66	43.28	18.69	/

Figure 4. Histogram of the overburden.

4.2. Engineering Case of the CFSHS-Based Height Calculation Method

According to the CFSHS-based height calculation method as well as Equations (1) and (2), the load and position of the bearing stratum in the overburden were calculated; the hard stratum and its bearing soft stratum were named from bottom to top. With reference to Equation (12), the free space height Δ_i under the stratum was calculated, and the results are listed in Table 1.

Table 1. Determination of the bearing stratum.

Number of the Stratum	Lithology	Thickness/m	Height from the Coal Seam Roof/m	Δ_i /m
1	Limestone	7.50	7.50	3.08
2	Mudstone	6.13	13.63	2.76
3	Sandy mudstone	3.17	16.80	2.49
4	Limestone	4.79	21.59	2.09
1st hard stratum	Mudstone	7.49	29.08	1.50
(1, 1) soft stratum	Fine sandstone	2.87	31.95	1.29
(1, 2) soft stratum	Limestone	3.25	35.20	1.05
2nd hard stratum	Fine sandstone	5.98	41.18	0.63
3rd hard stratum	Siltstone	8.38	49.56	0.05
(3, 1) soft stratum	Fine sandstone	5.77	55.33	−0.32
(3, 2) soft stratum	Siltstone	7.53	62.86	−0.80
(3, 3) soft stratum	Mudstone	4.13	66.99	−1.06
(3, 4) soft stratum	Limestone	5.20	72.19	−1.38
4th hard stratum	Sandy mudstone	9.48	81.67	−1.94

Based on the mechanical parameters of hard strata and the above Equations (5)–(8) and (11), L_z , θ , L_c and ω_{max} of hard strata can be obtained (Table 2).

Table 2. Calculated parameters of hard strata.

Number of the Stratum	L_z /m	$\theta/^\circ$	L_c /m	ω_{max} /mm
1st hard stratum	24.9	3.5	61.0	9.6
2nd hard stratum	24.5	1.5	60.0	10.0
3rd hard stratum	29.7	0.1	72.6	12.5
4th hard stratum	22.9	/	56.0	4.3

The height of the cavity below the first stratum is 1.50 m, and the bending subsidence deformation before the initial breakage is 9.6 mm. They were substituted in Equation (18) to determine whether that the first hard stratum breaks. Next, the parameters of the first hard stratum were substituted into Equations (3) and (4) to determine whether the first hard stratum can form a stable masonry beam structure. Therefore, the first hard stratum is the boundary stratum under the fracture zone, and the height of the caving zone is the height of the first hard stratum from the coal seam, which is 21.59 m.

The above steps were repeated on the 2nd, 3rd and 4th hard strata. Since the mining coal seam is thick and the 2nd and 3rd hard strata are close to the coal seam, cavities still exist under the 2nd and 3rd hard strata, whose heights are greater than its bending subsidence deformation value. Therefore, the 2nd and 3rd hard strata break, and the overburden failure continues to develop upward. In judging the 4th hard stratum, the cavity under the 4th hard stratum has been filled, which prevents the bending deformation of the 4th hard stratum from occurring, so the 4th hard stratum will not be damaged. Preliminary judgment holds that the height of the overburden failure in the working face 15,101 is between the 3rd and the 4th hard strata, i.e., 49.56–81.67 m.

In summary, there are four soft strata between the 3rd and the 4th hard strata. The four soft strata were judged from bottom to top with reference to Equations (15) and (16). It can be concluded that when the (3, 1) soft stratum is under load, its deflection value is not smaller than the free space height below it, so the soft stratum does not break, and the fracture development stops. Therefore, the (3, 1) soft stratum is the boundary stratum of the bending subsidence zone.

In addition, to explain the relationship between the free space height and the stratum height below the stratum more intuitively, Figure 5 gives the relationship curve between the free space height and the stratum height. The WCFZ develops to the 3rd hard stratum,

and the intersection of the curve and the horizontal axis is the maximum development height (49.56 m) of the WCFZ.

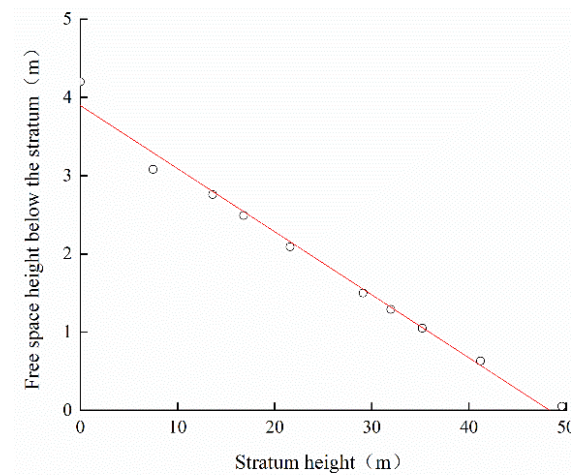


Figure 5. Relationship curve between the free space height below the stratum and the stratum height.

In conclusion, according to the proposed method, the height of the caving zone above the working face 15,101 of coal mine XJ is 21.59 m, and the development height of the WCFZ is 49.56 m. The (3, 1) soft stratum and its above strata belong to the bending subsidence zone (227.32 m thick).

4.3. Engineering Measurement and Analysis

4.3.1. Observation Scheme Design

Abundant aquifers exist in the overburden of most working faces in the mine. Considering this fact, with the working face 15,101 as an engineering case, the height of the WCFZ was detected and analyzed by a borehole television, and the development law of the WCFZ was analyzed by numerical simulation, which provided a basis for safe mining.

According to the theoretical calculation results, the development height of the WCFZ in the working face 15,101 is 49.56 m, so attention should be paid to the observation of fracture development in this range and the development of the WCFZ to the maximum value consumes 1–3 months. Therefore, considering the actual situation of the working face, the observation date is 43 days after recovery, and the observation site is located in the transportation lane of the working face 15,102, which is about 700 m away from the stopping line. The location of the drilling site is shown in Figure 6, and the drilling parameters are listed in Table 3.

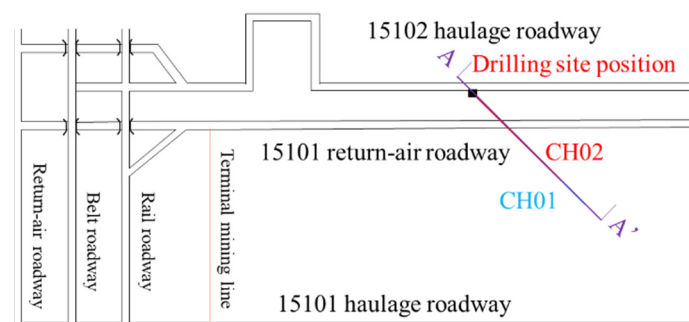


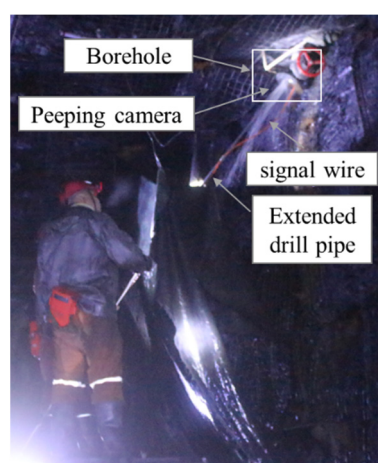
Figure 6. Plan of the drilling site position.

Table 3. Drilling parameters.

Borehole Number	Diameter/mm	Elevation/(°)	Azimuth/(°)	Hole Depth/m	Vertical Depth/m
CH01	Φ89	50	N137	118	90
CH02	Φ89	55	N137	110	90

4.3.2. Observation Method

This observation adopted the borehole television from Tianchen Geophysical Exploration Company (Wuhan, China) to visually measure the development of the WCFZ. The borehole television is composed of a peeping camera, a recorder, an extended drill pipe and an imager. During observation, the camera and the imager are connected through a signal wire; the camera then extends to the depth of the borehole by the extended drill pipe to transmit the images of fracture development in the borehole (Figure 7, an on-site photo).

**Figure 7.** Measured photo of the underground WCFZ.

4.3.3. Analysis on the Observation Results

Figure 8 shows the observation results of mining overburden fractures through the CH02 Borehole. The figures in the right bottom of photos are the distances from the camera to the borehole orifice, and the figures below are the vertical distances between the camera and the coal seam roof.

According to the on-site observation records, Figure 8a,b show the situations of mining overburden within the drilling depth of 12.52–19.78 m, which are 10.25–16.20 m high from coal seam 15 and are above the protective coal pillars between two adjacent working faces. The overburden sees no obvious mining-induced fracture, indicating that the borehole in this range has not entered the fracture zone. Figure 8c,d show the situations of mining overburden with the drilling depth of 30.38–36.30 m, which are 24.88–29.73 m high from coal seam 15. Notable mining-induced fractures begin to emerge in the overburden, and become increasingly obvious as the drilling is approaching the goaf center. The stratum in Figure 8d is seriously damaged; Figure 8e,f illustrate the situations of mining overburden within the drilling depth of 41.33–48.07 m, which are 33.85–39.37 m high from the coal seam 15. Obvious mining-induced fractures can be observed in the strata in this range, suggesting that the strata are significantly affected by mining. However, compared with the overburden of 36.30 borehole depth, the overburden of the drilling depth of 41.33–48.07 m are less damaged and present a certain regularity, and obvious separation occurs at the junction of some adjacent strata. Figure 8g,h show the situations of mining overburden within the drilling depth of 55.37–61.28 m, which are 45.35–50.19 m high from coal seam 15. According to the detection results, as the height from the coal seam increases, fractures become less developed. The distance and the development degree of fractures are negatively correlated, that is, in this range, the influence of mining on the strata weakens as the height from the

coal seam increases. When the borehole depth reaches 69.08 m (Figure 8i), that is, when the height from the roof of coal seam 15 is greater than 56.58 m, no obvious mining-induced fracture is found in the rock stratum. With the continuous advancement of the probe, when the borehole depth reaches 74.24 m (Figure 8j), i.e., when the height from the roof of coal seam 15 is beyond 60.08 m, no obvious mining-induced fracture is detected. In summary, the mining overburden of the working face 15,101 develops to 69.08 m borehole depth, and the distance from the roof of coal seam 15 is 56.58 m, that is, the height of the WCFZ detected by the CH02 Borehole is 56.58 m.

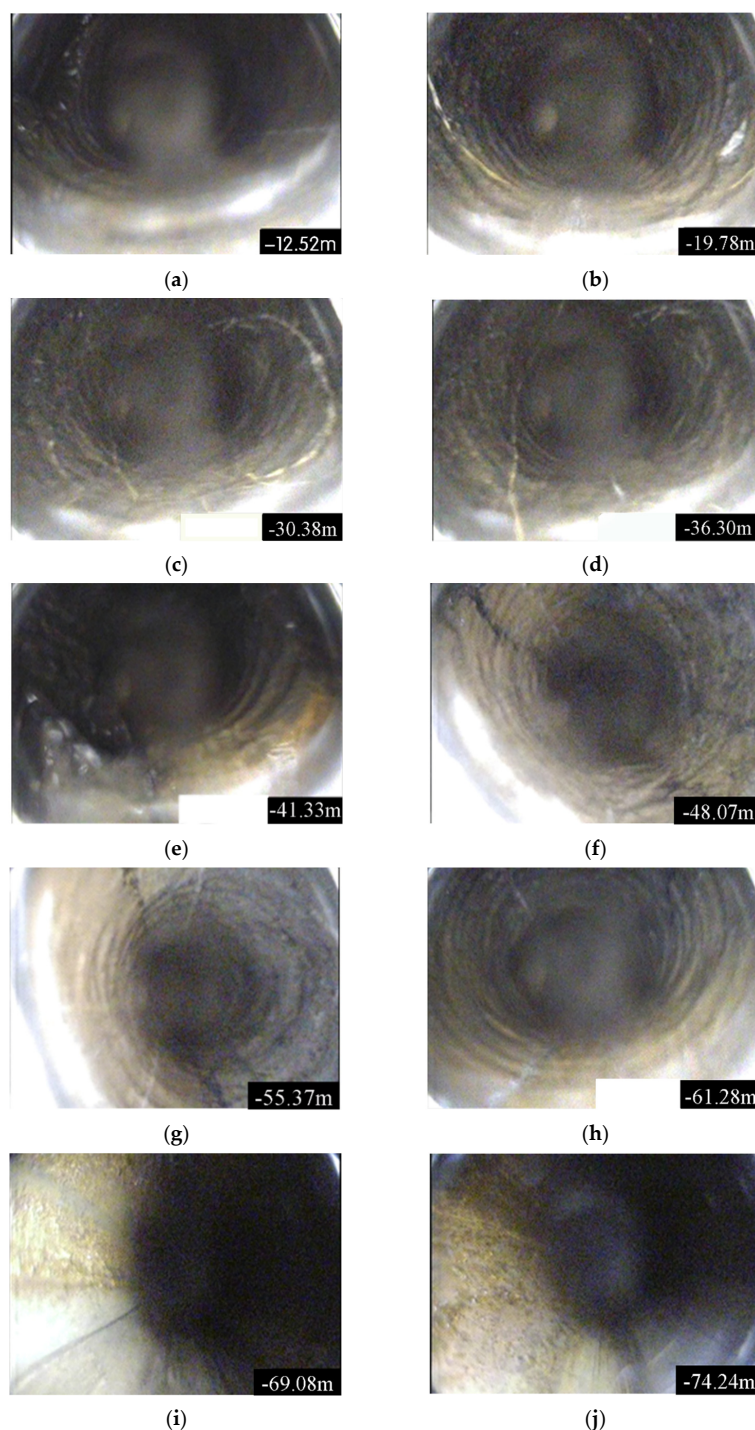


Figure 8. Photos of the overburden fractures after mining. (a) 10.25 m (b) 16.20 m (c) 24.88 m (d) 29.73 m (e) 33.85 m (f) 39.37 m (g) 45.35 m (h) 50.19 m (i) 56.58 m (j) 60.08 m.

Based on the measured results, the height of the caving zone in the goaf of the 15,101 working face is 29.73 m; the height of the WCFZ is 56.58 m; and the thickness of the bending subsidence zone is 220.30 m.

Then the calculation results of the above theoretical judgment method of the “vertical three zones” of mining overburden were contrastively analyzed with the on-site measured results. It can be found that the calculation results of the theoretical judgment method (the height of the caving zone 21.59 m, the development height of the WCFZ 49.56 m, and the thickness of the bending subsidence zone 227.32 m) are similar to the measured results, which verifies the rationality and practicability of the theoretical judgment method.

4.4. Numerical Simulation Analysis

To verify the rationality of the above analytical results, the geological mining conditions of the fully mechanized mining face 15,101 in coal mine XJ served as the background to simulate the caving and fracture characteristics of the mining overburden, and the migration process of the overburden failure was simulated by 3DEC discrete element simulation software.

4.4.1. Model Design

Based on the actual mining data of the fully mechanized face 15,101 in coal mine XJ, a 3DEC numerical calculation model was established. The advancing length of the working face is 420 m, which is extended outward by 180 m along the working face to prevent the influence of the model boundary on the calculation results. The model size is 600 m × 1 m × 300 m (length × width × height) (Figure 9). The simulated working face was excavated by 30 m each time, a total of 14 excavations.

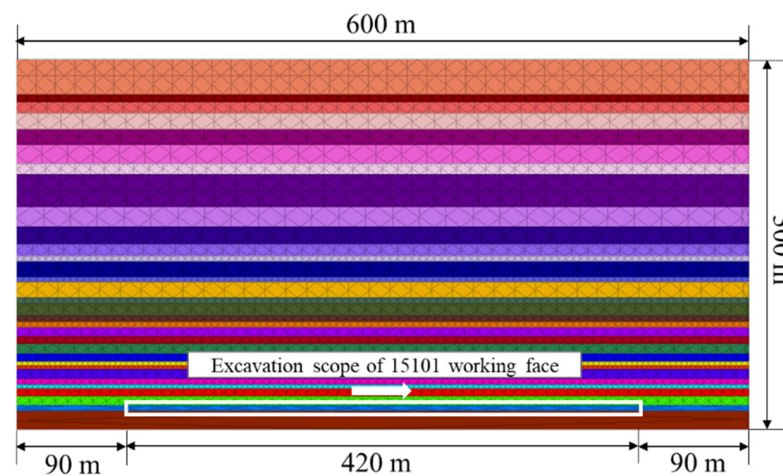


Figure 9. 3DEC numerical calculation model.

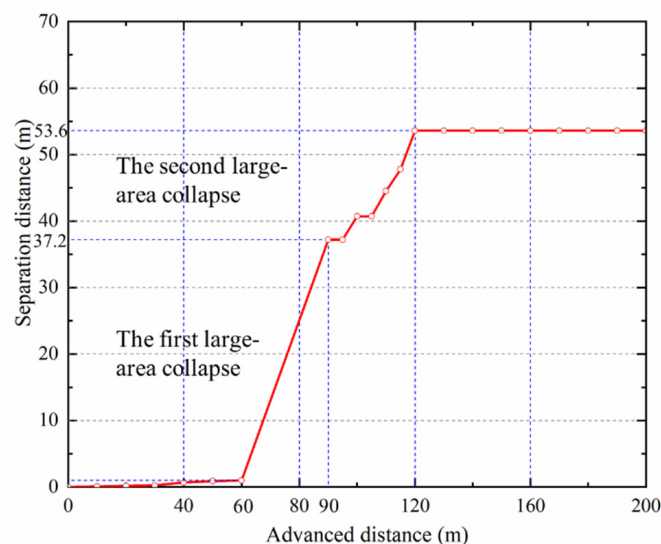
In the numerical model, the Mohr-Coulomb model was selected as the block constitutive model, and the Coulomb slip model was selected as the joint constitutive model. The left and right boundaries of the model were fixed in x direction displacement, the front and rear boundaries fixed in y direction displacement and the bottom boundary fixed in z direction displacement. According to the experimental data and model calibration, the physical and mechanical parameters of the overburden were determined (Table 4).

Table 4. Physical and mechanical parameters of the strata.

Lithology	Density /kg·m ⁻³	Bulk Modulus /GPa	Shear Modulus /MPa	Cohesion /MPa	Internal Friction Angle /°	Tensile Strength /MPa	Normal Stiffness /GN·m ⁻¹	Tangential Stiffness /GN·m ⁻¹
Loess	1832	0.28	0.093	0.85	25	0.35	0.25	0.25
Mudstone	2540	1.23	1.06	2.16	24	1.26	0.18	0.18
Sandy mudstone	2580	3.72	1.62	3.53	25	2.06	0.59	0.59
Medium grained sandstone	2630	2.31	1.26	5.92	26	2.86	0.50	0.50
Siltstone	2580	2.98	1.88	4.28	23	2.55	1.09	1.09
Fine sandstone	2610	2.64	1.68	4.36	22	2.32	0.49	0.49
Coal	1400	1.16	0.73	1.54	22	1.03	0.21	0.21
Limestone	2800	4.45	8.91	4.20	39	3.10	2.60	2.60

4.4.2. Simulation Results and Analysis

With the advancement of the working face, the caving form of the overburden is shown in Figure 10. When the working face advances to 90 m (Figure 11a), the overburden begins to cave in a large area, with 4.39 m maximum vertical displacement; the broken limestone forms a masonry beam structure. At this time, the overburden above the coal seam is separated, with 37.2 m separation height. When the working face advances to 120 m (Figure 11b), the overburden further migrates in a large area, and the separation develops upward to 53.6 m. When the working face advances to 150 m (Figure 11c), the lower separation layer is closed. When the working face is excavated to 420 m (Figure 11d), the separation layer does not develop upward further; according to the closure state of the vertical fractures in Figure 12 (the red and green represent open and closed fractures respectively), the following conclusions can be obtained: (1) when the working face 15,101 reaches the full mining state in the advancing direction, the overburden migrates and the fractures are closed again; in the goaf middle, the number of closed fractures decreases from the middle to the edge, and the fractures display a “V” shape on the edges of both goaf sides. (2) The vertical interpenetrated fractures of the overburden finally develop to the 53.6 m fine sandstone above the coal seam.

**Figure 10.** Overburden failure characteristics with different excavation steps.

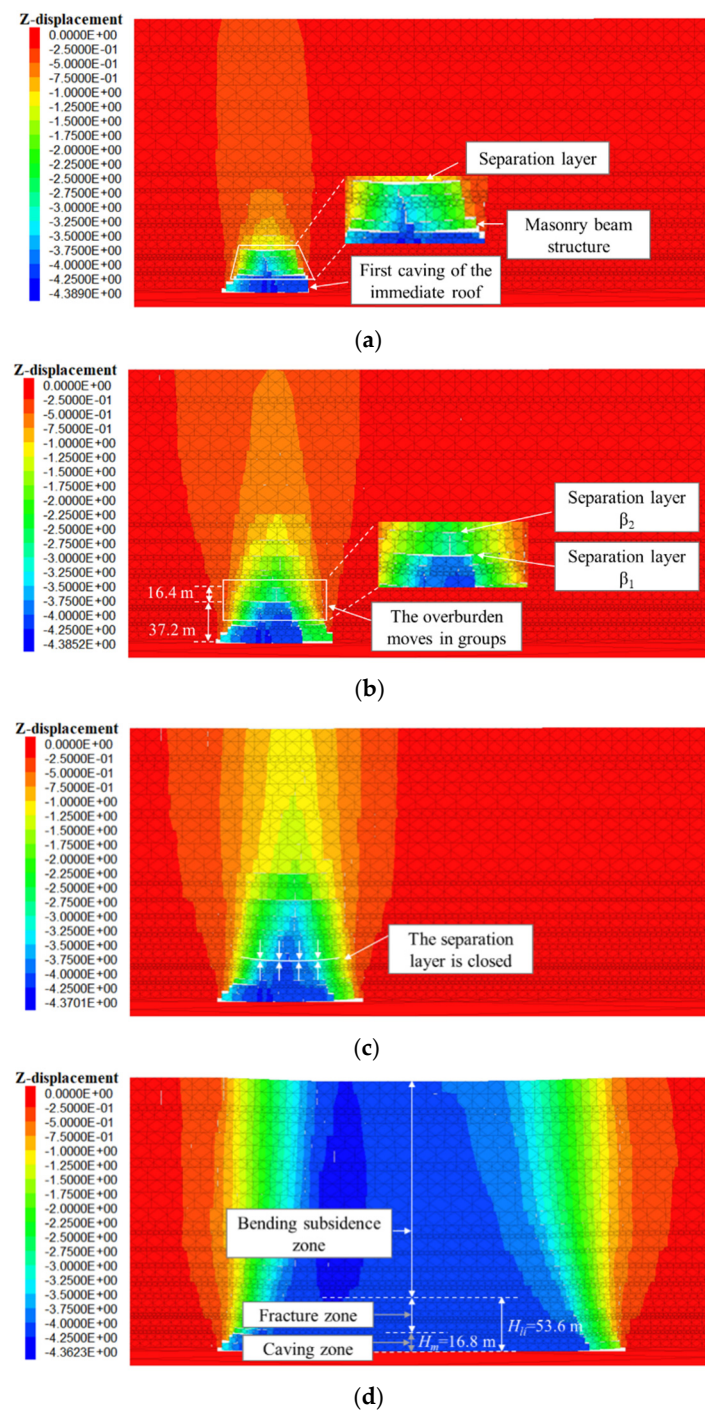


Figure 11. Nephograms of vertical displacement of the overburden during the advancement of working face. (a) Excavation to 90 m; (b) Excavation to 120 m; (c) Excavation to 150 m; (d) Excavation to 420 m.

The above numerical simulation experiment leads to the following conclusions: (1) Overburden failure migrates upward in the form of separation layer. When the bending deformation of the stratum below the separation reaches its deformation limit, it interpenetrates the vertical fractures of the overburden, and finally forms a complete overburden water-conducting channel. (2) The upward development of the overburden failure is affected by the hard stratum, so the overburden moves in groups. (3) The numerical simulation reveals that the water-conducting fracture zone is 53.6 m high.

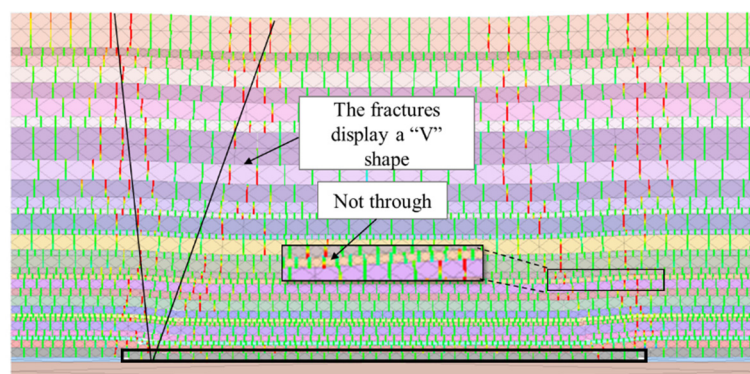


Figure 12. Closure state of the vertical fractures.

4.5. Scope of Application

This model is a theoretical model, and the application of this model is limited. When the movement of strata above gob is only affected by self-weight and overburden pressure, this model is applied well. But when a place has a wide range of geological structure (e.g., fault, folds) or geological events (e.g., earthquake), this model will be not suitable.

5. Conclusions

(1) The structure of mining overburden failure in the coal mine was analyzed, and the mechanical model of overburden structure conduction was established. The results suggest that the height of overburden failure is controlled by the lithology of soft strata between adjacent hard strata and the height of free space below.

(2) The bearing stratum breakage distance, maximum deflection and free space of overburden were studied with reference to the overburden histogram data. On this basis, the CFSHS-based height calculation method was proposed, and its applicable conditions were given.

(3) Through the engineering field test, the height of overburden failure in the working face was investigated by means of field measurement and numerical simulation. Moreover, the results obtained through the CFSHS-based height calculation method, numerical simulation and field measurement were comparatively analyzed. The comparison verified accuracy of the CFSHS-based height calculation method.

Author Contributions: Conceptualization, Y.T. and H.C.; methodology, W.Y.; software, W.L. and W.Y.; validation, S.W. and Y.X.; formal analysis, W.G.; investigation, D.Y. and W.Y.; resources, T.Q.; data curation, Y.T. and J.R.; writing—original draft preparation, Y.T.; writing—review and editing, W.Y.; visualization, W.G.; supervision, W.Y.; project administration, Y.Z.; funding acquisition, Y.T. All authors have read and agreed to the published version of the manuscript.

Funding: This work was financially supported by National Natural Science Foundation of China (U21A20108, 52174108, 51974105 and 52104127), Support Plan for Science & Technology Innovation Talents in Universities of Henan Province (21HASTIT024), State Key Laboratory of Coal Resources in Western China (SKLCRKF1912), Scientific and technological innovation research team of Henan Polytechnic University (T2021-5), Henan Excellent Youth Science Foundation (222300420045), Henan Science and Technology Research Project (212102310399, 222102320058), Key Scientific Research Projects of Colleges and Universities in Henan Province (21A440003).

Institutional Review Board Statement: Not applicable.

Informed Consent Statement: Not applicable.

Data Availability Statement: Not applicable.

Acknowledgments: The authors gratefully acknowledge the editor and reviewers for their helpful comments.

Conflicts of Interest: The authors declare no conflict of interest.

References

1. Peng, S.S. *Coal Mine Ground Control*; Wiley: New York, NY, USA, 1978.
2. Kratzsch, H. *Mining Subsidence Engineering*; Springer: Berlin/Heidelberg, Germany, 1983.
3. Gray, R.E. Mining subsidence- past, present, future. *Int. J. Min. Geol. Eng.* **1990**, *8*, 400–408. [[CrossRef](#)]
4. Kang, Y.; Jin, R. Actuality and developing trend of long wall top coal caving mining under water. *Coal Min. Technol.* **2003**, *1*, 15–18.
5. Yan, W.; Chen, J.; Yang, W.; Liu, X.; Wang, W.; Zhang, W. On-Site Measurement on Surface Disturbance Law of Repeated Mining with High Relief Terrain. *Sustainability* **2022**, *14*, 3166. [[CrossRef](#)]
6. Fan, G.; Zhang, D.; Ma, L. Overburden movement and fracture distribution induced by longwall mining of the shallow coal seam in the Shendong coalfield. *J. China Univ. Min. Technol.* **2011**, *40*, 196–201.
7. State Administration of Safety; State Administration of Coal Mine Safety; State Energy Administration; State Railway Administration. *Buildings Water, Railways and Main Well Lane of Coal Pillar and Mining Regulations*; China Coal Industry Publishing House: Beijing, China, 2017.
8. Sun, Y.; Xu, Z.; Dong, Q. Monitoring and simulation research on development of water flowing fractures for coal mining under Xiaolangdi reservoir. *Chin. J. Rock Mech. Eng.* **2011**, *31*, 3444–3451.
9. Cao, D.; Li, W. Estimation method for height of fractured zone with in coal mining area. *Chin. J. Geol. Hazard Control* **2014**, *1*, 63–69.
10. Vervoor, A. Various phases in surface movements linked to deep coal longwall mining: From start-up till the period after closure. *Int. J. Coal Sci. Technol.* **2021**, *8*, 412–426. [[CrossRef](#)]
11. Guo, C.; Yang, Z.; Li, S.; Lou, J. Predicting the Water-Conducting Fracture Zone (WCFZ) Height Using an MPGA-SVR Approach. *Sustainability* **2020**, *12*, 1809. [[CrossRef](#)]
12. Wanner, C.; Bucher, K.; von Strandmann, P.A.P.; Waber, H.N.; Pettke, T. On the use of Li isotopes as a proxy for water–rock interaction in fractured crystalline rocks: A case study from the Gotthard rail base tunnel. *Geochim. Cosmochim. Acta* **2017**, *198*, 396–418. [[CrossRef](#)]
13. Khanzode, V.V.; Maiti, J.; Ray, P.K. A methodology for evaluation and monitoring of recurring hazards in underground coal mining. *Saf. Sci.* **2011**, *49*, 1172–1179. [[CrossRef](#)]
14. Rezaei, M.; Hossaini, M.F.; Majdi, A. A time-independent energy model to determine the height of distressed zone above the mined panel in longwall coal mining. *Tunn. Undergr. Space Technol.* **2015**, *47*, 81–92. [[CrossRef](#)]
15. Xu, Y.; Li, J.; Liu, S.; Zhou, L. Calculation formula of “two-zone” height overlying strata and its adaptability analysis. *Coal Min. Technol.* **2011**, *2*, 4–7.
16. Xu, Y.; Liu, S. Study on method to set safety coal and rock pillar for full mechanized top coal caving mining under water body. *Coal Sci. Technol.* **2011**, *11*, 1–4.
17. Qian, M.; Miao, X. Theoretical analysis of the structural form and stability of overlying strata in Long wang mining. *Chin. J. Rock Mech. Eng.* **1995**, *2*, 97–106.
18. Guo, H.; Sun, Z.; Ji, M.; Wu, Y.; Nian, L. An Investigation on the Impact of Unloading Rate on Coal Mechanical Properties and Energy Evolution Law. *Int. J. Environ. Res. Public Health* **2022**, *19*, 4546. [[CrossRef](#)] [[PubMed](#)]
19. Wang, Y.; Wang, X.; Zhang, J.; Chen, X.; Zhu, W.; Zhang, Y. Roof Subsidence and Movement Law of Composite Strata Mining: Insights from Physical and Numerical Modeling. *Minerals* **2022**, *12*, 3. [[CrossRef](#)]
20. Zhai, W.; Li, W.; Huang, Y.; Ouyang, S.; Ma, K.; Li, J.; Gao, H.; Zhang, P. A Case Study of the Water Abundance Evaluation of Roof Aquifer Based on the Development Height of Water-Conducting Fracture Zone. *Energies* **2020**, *13*, 4095. [[CrossRef](#)]
21. Sun, Q.; Mu, Y.; Yang, X. Study on “two zones” height of overlying of fully-mechanized technology with high mining height at Hongliu Coal Mine. *J. China Coal Soc.* **2013**, *38*, 283–286.
22. Xun, Y. Research on movement and evolution law of breaking of overlying strata in shallow coal seam with a thin bedrock. *Rock Soil Mech.* **2008**, *2*, 512–516.
23. Yan, W.; Chen, J.; Tan, Y.; Zhang, W.; Cai, L. Theoretical Analysis of Mining Induced Overburden Subsidence Boundary with the Horizontal Coal Seam Mining. *Adv. Civ. Eng.* **2021**, *2021*, 6657738. [[CrossRef](#)]
24. Sun, Y.; Zuo, J.; Karakus, M.; Liu, L.; Zhou, H.; Yu, M. A New Theoretical Method to Predict Strata Movement and Surface Subsidence due to Inclined Coal Seam Mining. *Rock Mech. Rock Eng.* **2021**, *54*, 2723–2740. [[CrossRef](#)]
25. Thongprapha, T.; Fuenkajorn, K.; Daemen, J.K. Study of surface subsidence above an underground opening using a trap door apparatus. *Tunn. Undergr. Space Technol.* **2015**, *46*, 94–103. [[CrossRef](#)]
26. Vervoort, A. Surface movement above an underground coal longwall mine after closure. *Nat. Hazards Earth Syst. Sci.* **2016**, *9*, 2107–2121. [[CrossRef](#)]
27. Sasaoka, T.; Takamoto, H.; Shimada, H.; Oya, J.; Hamanaka, A.; Matsui, K. Surface subsidence due to underground mining operation under weak geological condition in Indonesia. *J. Rock Mech. Geotech. Eng.* **2015**, *3*, 337–344. [[CrossRef](#)]
28. Mokhov, A.V. A rock mass permeability model within the subsidence zone in workings of coal fields. *Dokl. Earth Sci.* **2017**, *473*, 390–393. [[CrossRef](#)]
29. Yang, W.; Guo, W.; Zhao, G.; Ma, Z.; Yang, D. Theoretical judgement method of overburden “Three-zone” based on rock strata deflection deformation and its engineering application. *Coal Sci. Technol.* **2021**, 1–9. Available online: <http://kns.cnki.net/kcms/detail/11.2402.TD.20211206.2350.003.html> (accessed on 17 March 2022).
30. Hou, E.; Wen, Q.; Ye, Z.; Chen, W.; Wei, J. Height prediction of water-flowing fracture zone with a genetic-algorithm support-vector-machine method. *Int. J. Coal Sci. Technol.* **2020**, *7*, 740–751. [[CrossRef](#)]

31. Cao, Z.; Ju, J.; Xu, J. Distribution model of water-conducted fracture main channel and its flow characteristics. *J. China Coal Soc.* **2019**, *12*, 3719–3728.
32. Gao, B.; Wang, X.; Zhu, M.; Zhou, J. Dynamic development characteristics of two zones of overburden strata under conditions of compound roof highly gassy and thick coal seam in full-mechanized top coal caving faces. *Chin. J. Rock Mech. Eng.* **2013**, *31*, 3444–3451.
33. Cao, J.; Ma, Q.; Wang, Y. Study of Wide Strip Mining Based on Spatial Structure Principle of Overlying Strata. *Coal Sci. Technol.* **2008**, *1*, 68–72.